IET Power Electronics

Research Article

IET Journals
The Institution of Engineering and Technology

Robust integral controllers for high-order class-D power amplifiers

ISSN 1755-4535
Received on 15th June 2017
Revised 24th October 2017
Accepted on 22nd November 2017
doi: 10.1049/iet-pel.2017.0441
www.ietdl.org

Gunyaz Ablay[1] ✉

[1]*Electrical–Electronics Engineering Department, Abdullah Gül University, Kayseri, Turkey*
✉ *E-mail: gunyaz.ablay@agu.edu.tr*

Abstract: This study presents variable structure system theory based robust integral controllers for class-D power amplifiers. These amplifiers are highly efficient switching type power amplifiers with negligible losses. Sensorless and current feedback based integral controllers with sliding modes are designed to provide robust tracking performance with negligible phase delays and distortions. The methods are capable of providing high-quality outputs by maximising gain and minimising the tracking error and phase shifts. The validity, feasibility and robustness performance of the controllers are investigated through circuit realisations.

1 Introduction

Class-D power amplifiers have been getting a great deal of interest in the industry in recent years due to their low power dissipation, high efficiency, small circuit board space, low cost and extended battery life. They have acquired a significant place in many electronic applications, e.g. portable devices, television sets, and theatres, and entered into the automotive and mobile audio systems [1, 2].

The control of the class-D power amplifiers has been studied well in the literature. The available amplifier control techniques utilise the Pulse-width modulators (PWMs) [3–5] and hysteretic (pulse density) modulators [6–8]. Performance in terms of low distortion, noise, and dynamic range differs significantly with the modulator topology used. While an improvement on the PWM based controllers is still existed [9–13], the most important studies are based on the hysteretic modulators. In general, the highest system performance with respect to low distortion, noise, and dynamic range is obtained with analogue hysteretic modulators due to the continuous time operation and non-quantised resolution [14]. The main advantages of the hysteretic modulators include self-oscillating modulation (no need any external carrier signal), linear modulation with sawtooth-shaped carrier, infinite power supply rejection ratio and simple design. Due to these benefits, recently some advanced control designs based on hysteretic modulation have been proposed including self-oscillating amplifiers [15–17], sigma-delta modulation based control [8, 18, 19], hysteresis controller [14, 20, 21], bang-bang control [22], and sliding mode control [23–27]. These methods allow simple and stable designs, but, in general, can result in up to π phase delay between the input and output and low switching frequency causing harmonic oscillations in the output.

In this work, a sensorless control approach and a current feedback control method with hysteretic modulators are studied. The theory behind the approaches is established using variable structure system theory for high-order class-D amplifiers. The controllers are capable of providing good stability conditions for any load conditions. A fast dynamic response and high switching frequency can be set via the design of control gains without increasing system complexity. In the following sections, the design approach of controllers and their circuit implementations and results are provided.

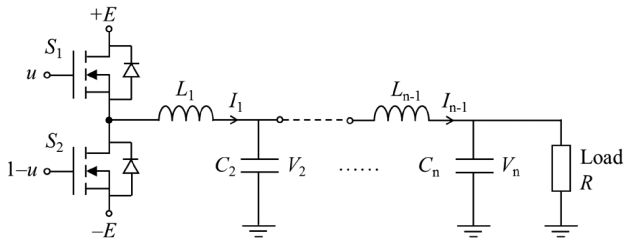

Fig. 1 *Nth order class-D power amplifier*

2 High-order class-D power amplifiers

A class-D amplifier acts as a voltage amplifier with very high input impedance and very low output impedance and can provide higher than 90% efficiency at full power and a very high output power. These power amplifiers can be designed with half-bridge and full-bridge configurations. The single-ended half bridge structure minimises the number of LC filter components required per channel and more suitable for closed-loop control designs compared with the full-bridge topology. The closed-loop control is necessary for low cost and high performance applications.

The LC filter is necessary to eliminate electromagnetic interference and high-frequency power dissipation. The quality of the low-pass filtering can be enhanced with the increased number of LCs (by reducing output harmonics) for higher-power systems. However, the system degree increases with the number of LCs, which causes difficulty in the control designs. An nth order class-D power amplifier can be built with nth order LC filters as shown in Fig. 1.

The switches of the amplifier work in complementary states to avoid power supply internal short circuits. To facilitate the system analysis and control design, the parasitic elements, switch delays, switch voltage drops and auxiliary networks may be neglected. Considering the circuit shown in Fig. 1, the model of the nth order class-D amplifier is obtained as

$$\begin{aligned} L_1\dot{I}_1 &= -V_2 + (2u-1)E, \\ C_i\dot{V}_i &= I_{i-1} - I_{i+1}, \\ L_{i+1}\dot{I}_{i+1} &= V_i - V_{i+2}, \\ &\vdots \\ C_n\dot{V}_n &= I_{n-1} - V_n/R, \end{aligned} \tag{1}$$

where inductor currents, I_i, and capacitor voltages, V_i, are the state variables of the system for $i = 2, 4, \ldots, n-2$, R is the load resistance, E is the supply voltage, u is the control signal taking only discrete values $u \in \{0, 1\}$, and L_i, C_i are the inductances and capacitances of the filter elements.

The control objective is to track the reference signal V_r during the equilibrium. The equilibrium point is calculated by setting all time derivatives of the state variables to zero, i.e., $\dot{I}_j = \dot{V}_{j+1} = 0$ (for $j = 1,\ 3, \ldots, n-1$). For the model (1), the average equilibrium point for a desired output voltage, $V_n = V_r$, can be written as

$$I_j^* = V_r/R, \quad V_{j+1}^* = V_r, \quad u^* = (V_r + E)/2E\,. \tag{2}$$

Since the control input must remain constant during the steady-state, the average control can be used in the equilibrium solutions. Since $u \in \{0, 1\}$, the steady-state value of the average control signal must satisfy

$$0 < u^* < 1. \tag{3}$$

Thus, from (2) and (3), it is clear that the reference V_r must be smaller than the supply voltage, i.e. $-E < V_r < E$. A fast switching non-linear control method is needed for providing a fast dynamic response, small phase delay, and robustness against load variations.

3 Robust integral control designs for class-D amplifiers

In this work, an integral switching controller is designed under the variable structure control theory for robust solutions. Variable structure control with sliding modes which is a natural switch-mode controller is a good candidate to meet the control objectives of the class-D power amplifiers. The state dependent discrete input signals and robustness feature of sliding modes can lead to simple implementation advantage for such power amplifiers.

3.1 Sensorless control

The sensorless control means that the controller uses only voltage feedback without using any current sensing components. Consider an integral switching manifold based switching controller

$$u = \begin{cases} 1, & \text{if } s > 0, \\ 0, & \text{if } s < 0, \end{cases} \tag{4}$$

$$s = \beta \int_0^t (V_r(\tau) - (2u-1)E)\ \mathrm{d}\tau, \tag{5}$$

where V_r is a reference signal and β is a positive control parameter (integrator time constant in practice). To investigate the effect of average control, when $\dot{s} = 0$, the related control signal is found as

$$u_{ave} = (V_r + E)/2E\,. \tag{6}$$

The average control (or equivalent control) can be obtained through a first-order low pass filter [28].

Under non-saturated operating conditions (with $-E < V_r < E$), the average control assures

$$0 < u_{ave} < 1. \tag{7}$$

Substituting (6) into (1), the resulting ideal system dynamics (zero dynamics) for the fourth-order class-D amplifier can be written as

$$\begin{bmatrix} \dot{I}_1 \\ \dot{V}_2 \\ \dot{I}_3 \\ \dot{V}_4 \end{bmatrix} = \begin{bmatrix} 0 & -\delta_1 & 0 & 0 \\ 1/C_2 & 0 & -1/C_2 & 0 \\ 0 & 1/L_3 & 0 & -1/L_3 \\ 0 & 0 & 1/C_4 & -1/RC_4 \end{bmatrix} \begin{bmatrix} I_1 \\ V_2 \\ I_3 \\ V_4 \end{bmatrix} + \begin{bmatrix} \delta_1 \\ 0 \\ 0 \\ 0 \end{bmatrix} V_r, \tag{8}$$

where $\delta_1 = 1/L_1$. The system dynamics given in (8) have the equilibrium point, $I_1^* = I_3^* = V_r/R$ and $V_2^* = V_4^* = V_r$. The characteristic equation of (8) with the eigenvalue λ is

$$\lambda^4 + \frac{\lambda^3}{RC_4} + \frac{(C_2 + C_4)\lambda^2}{C_2C_4L_3} + \frac{\lambda}{RC_2C_4L_3} + \frac{1}{C_2C_4L_1L_3} = 0. \tag{9}$$

Since (9) has always negative real valued eigenvalues, the system dynamics given in (8) under the average control is asymptotically stable.

The stability of the feedback control system under the controller (4) and (5) can be evaluated through Lyapunov stability, i.e. for a positive definite function, $V = s^2/2 > 0$, stability is ensured if its time derivative is negative definite, $\dot{V} = s\dot{s} < 0$ [28]. From (5), for the reference, V_r, the time derivative of the switching manifold can be written as

$$\dot{s} = \beta(V_r - (2u-1)E)\,. \tag{10}$$

From (4), if $s > 0$ and $u = 1$, then $\dot{s} = \beta(V_r - E) < 0$ (since $-E < V_r < E$) and $s\dot{s} < 0$, so the system is stable. If $s < 0$ and $u = 0$, then $\dot{s} = \beta(V_r + E) > 0$ and $s\dot{s} < 0$, so the feedback system has stable dynamics. Consequently, the sensorless control strategy ensures that the system trajectory will stay on the desired reference at steady-state. The analysis can easily be extended to nth order class-D amplifiers since the LC filter is designed to have stable dynamics.

The sensorless control is simple, but it is not possible to enhance the response of the system dynamics with the controller gain, β, since it does not appear in the ideal system dynamics as seen in (8). For this reason, the following controller is proposed to improve the control performance of the nth order class-D amplifiers.

3.2 Current feedback based integral control

An effective switching control system for the nth order class-D power amplifier can be designed with a switching manifold as

$$u = \begin{cases} 1, & \text{if } s > 0, \\ 0, & \text{if } s < 0, \end{cases} \tag{11}$$

$$s = -I_1 + \beta \int_0^t (V_r(\tau) - V_n(\tau) - \gamma(2u-1)E)\ \mathrm{d}\tau, \tag{12}$$

where s is the switching manifold, V_r is the reference signal, β is a positive control gain, and γ is a positive constant defined by $0 \le \gamma < 1$. First, the effect of the average control is going to be analysed. From (12), when $\dot{s} = 0$, a corresponding average control is found as

$$u_{ave} = \frac{\beta L_1(V_r - V_n) + V_2 + (\beta\gamma L_1 + 1)E}{2(\beta\gamma L_1 + 1)E}. \tag{13}$$

The average control under non-saturating conditions satisfies

$$0 < u_{ave} < 1 \tag{14}$$

with $-(\beta\gamma L_1 + 1)E < \beta L_1(V_r - V_n) + V_2 < (\beta\gamma L_1 + 1)E$. For simplification of the analysis, now, consider a fourth-order class-D power amplifier. Under the average control (13), the ideal system dynamics (or zero dynamics) is obtained as

$$\begin{bmatrix} \dot{I}_1 \\ \dot{V}_2 \\ \dot{I}_3 \\ \dot{V}_4 \end{bmatrix} = \begin{bmatrix} 0 & -\delta_2 & 0 & -\delta_2 \\ 1/C_2 & 0 & -1/C_2 & 0 \\ 0 & 1/L_3 & 0 & -1/L_3 \\ 0 & 0 & 1/C_4 & -1/RC_4 \end{bmatrix} \begin{bmatrix} I_1 \\ V_2 \\ I_3 \\ V_4 \end{bmatrix} + \begin{bmatrix} \delta_2 \\ 0 \\ 0 \\ 0 \end{bmatrix} V_r, \tag{15}$$

where $\delta_2 = \beta\gamma/(\beta\gamma L_1 + 1)$. The ideal dynamics (15) has the equilibrium point, $V_2^* = V_4^* = V_r/(\gamma + 1)$ and $I_1^* = I_3^* = V_r/(\gamma + 1)R$, and if $\gamma \to 0$, then $V_4^* = V_r$. The characteristic equation of (15) for the eigenvalue λ can be written as

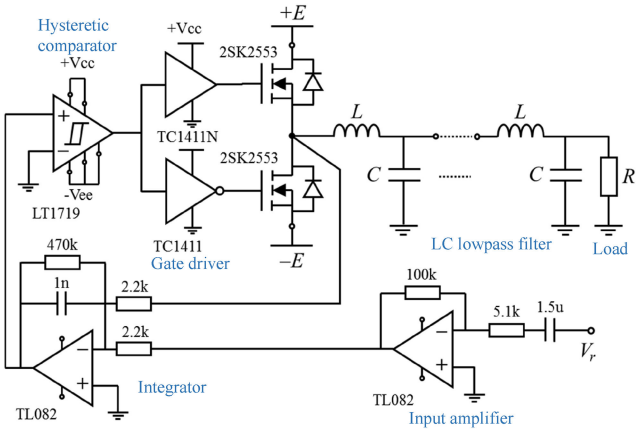

Fig. 2 *Circuit implementation of sensorless control scheme*

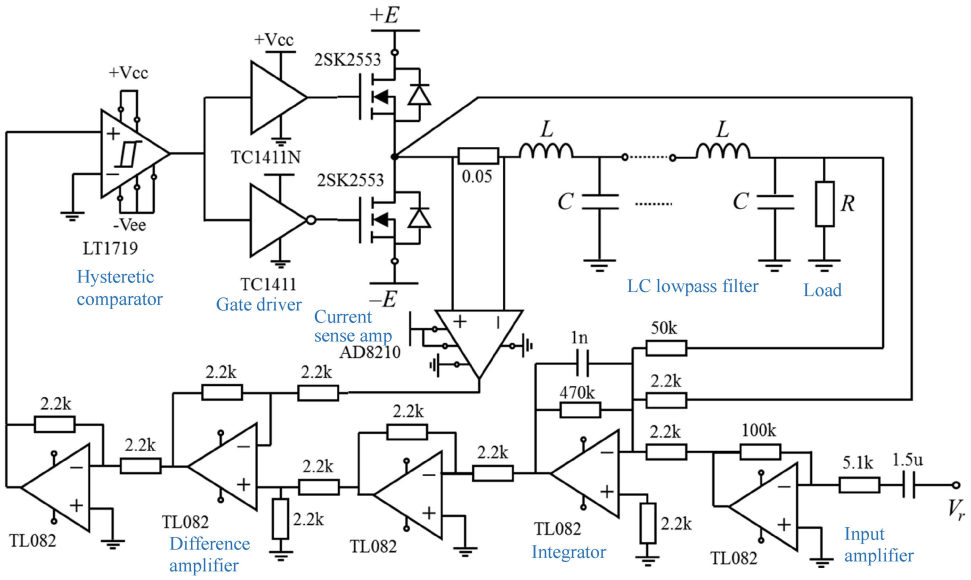

Fig. 3 *Circuit implementation of current feedback based control scheme*

$$\lambda^4 + \frac{1}{RC_4}\lambda^3 + \frac{C_2 + C_4 + \beta\gamma(C_2L_1 + C_4L_1 + C_4L_3)}{C_2C_4L_3(\beta\gamma L_1 + 1)}\lambda^2 + \frac{\beta\gamma L_1 + \beta\gamma L_3 + 1}{RC_2C_4L_3(\beta\gamma L_1 + 1)}\lambda + \frac{\beta(\gamma + 1)}{C_2C_4L_3(\beta\gamma L_1 + 1)} = 0. \tag{16}$$

By using the Routh's stability criterion for (16), the stability condition is found as

$$0 < \beta < 1/(L_3 - \gamma L_1)\,. \tag{17}$$

As long as the condition (17) is satisfied, the ideal system dynamics is always asymptotically stable for the fourth-order amplifier.

Finally, to analyse the stability of the closed-loop system under switching controller, for $V = s^2/2 > 0$, the time derivative of this function must satisfy $\dot{V} = s\dot{s} < 0$ for stability. From (12), for the reference, V_r, the time derivative of the switching manifold can be written as

$$\dot{s} = \beta(V_r - V_4) + [V_2 - (\beta\gamma L_1 + 1)(2u - 1)E]/L_1\,. \tag{18}$$

From (11), if $s > 0$ and $u = 1$, then $\dot{s} = \beta(V_r - V_4) + (V_2 - (\beta\gamma L_1 + 1)E)/L_1 < 0$ and $s\dot{s} < 0$. If $s < 0$ and $u = 0$, then $\dot{s} = \beta(V_r - V_4) + (V_2 + (\beta\gamma L_1 + 1)E)/L_1 > 0$ (due to the conditions given in (14) and (17)) and $s\dot{s} < 0$. Since the stability condition, $\dot{V} = s\dot{s} < 0$, is always satisfied, the closed-loop system is stable under the control (11) and (12).

To generalise the given stability analysis to the nth order class-D amplifier, if all LC filter components are designed to be equal, i.e. $L_j = L$ and $C_{j+1} = C$, then the stability condition for the nth order class-D power amplifiers is obtained as

$$\begin{aligned} &0 < \beta, \quad \text{if } n = 2, \\ &0 < \beta < 4.36/\left(n^{1.1}L(1-\gamma)\right), \quad \text{if } n = 4, 6, 8, \ldots \end{aligned} \tag{19}$$

To provide the desired control performance, the control gain β should be selected suitably by considering the stability condition (19).

3.3 Circuit realisations of controllers

A circuit implementation of class-D amplifiers with controllers can be composed of the output stage (switches and gate drivers), LC filter, difference amplifier, integrator and hysteretic comparator as shown in Figs. 2 and 3. The control and output stages can be realised with standard integrated circuit technology for high performances. In the design of the LC low-pass filter, the values of filter elements, L and C, are designed from the filter cut-off frequency (f_c) requirements given by

$$f_c = \left(\sqrt{2^{2/n} - 1}\right)/(2\pi\sqrt{LC}), \tag{20}$$

where n is the order of the filter ($n/2$ cascaded stages). A higher-order filter is designed to reduce the amount of harmonics without introducing a large phase shift. In the filter design, the Butterworth, Chebyshev and Bessel polynomials can be used to achieve suitable phase shift and ripple requirements. For a flat magnitude response within the given band, a Butterworth filter approximation with the

Table 1 Class-D amplifier design specifications and control performances

Class-D amplifier					Sensorless control				Current feedback control			
Amplifier order	LC values	Cut-off freq., f_c, kHz	Supply/ load	Reference signal freq., kHz	Time constant, R_lC_l, µs	Phase delay, °	THD, dB	Gain, %	Time constant, R_lC_l, µs	Phase delay, °	THD, dB	Gain, %
second order	60 µH, 0.47 µF	30	5 V, 8 Ω	10	2.2	25°	−48	100	2.2	15	−46	100
fourth order	43 µH, 0.27 µF	30	5 V, 8 Ω	10	2.2	35°	−48	91	2.2	23	−47	100
sixth order	33 µH, 0.22 µF	30	5 V, 8 Ω	10	2.2	39°	−46	88	2.2	26	−46	100

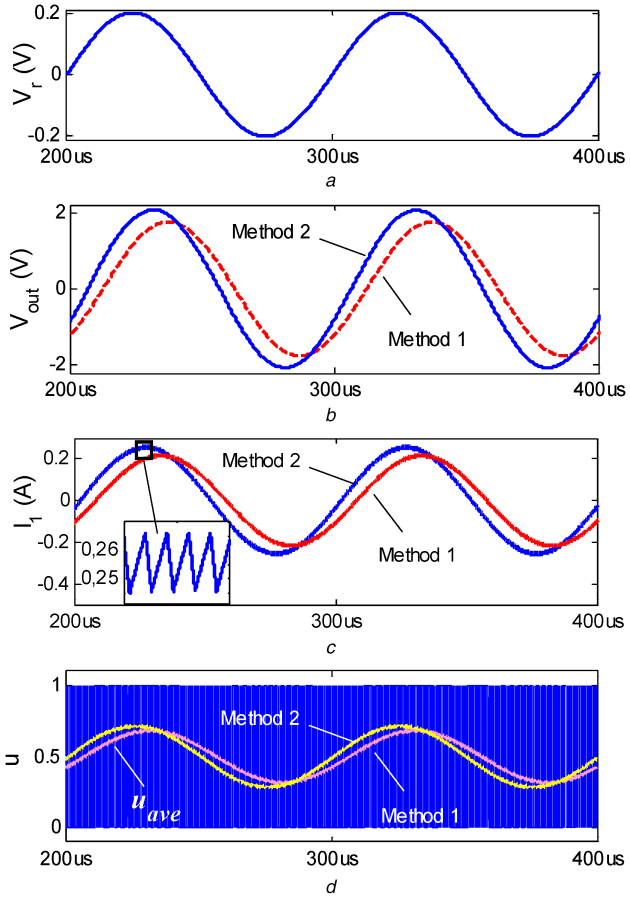

Fig. 4 *Numerical waveforms for the fourth-order amplifier*
(a) Reference input, ***(b)*** amplifier output for sensorless (method 1) and current feedback (method 2) controllers, ***(c)*** Inductor current, ***(d)*** Control signal with its average value

normalised characteristic equation, $\lambda^2+\sqrt{2}\lambda+1=\lambda^2+\lambda/RC+1/LC=0$, can be used to design LC filter parameters [29]. For a cut-off frequency $f_c=30$ kHz (or $\omega_c=2\pi f_c$) and a load resistance $R=8\ \Omega$, the LC values can be calculated as

$$C=1/(\omega_c\sqrt{2}R)=0.47\ \mu\text{F},\quad L=\sqrt{2}R/\omega_c=60\ \mu\text{H}. \tag{21}$$

For higher-order LC filters (i.e. fourth and sixth order), the calculated LC values are given in Table 1.

The amount of switching frequency can be controlled with integrator time constant and hysteresis band of the comparator. To get a low noise component at the amplifier output, the hysteresis band should be low, and it can be selected around $h=V_h/V_{DD}\le 0.02$, where the hysteresis of the comparator is given by $\pm V_h$. Note that a PWM comparator with a suitable switching frequency (e.g. 500 kHz) can also be used instead of a hysteretic comparator. In the integrator design, a fast transient response is considered. The integrator time constant is taken as $R_IC_I=2.2\ \mu$s. The input amplifier is an inverting amplifier with a gain of R_F/R_{IN}. The input must be ac coupled with a capacitor C_{IN}. This results in a high-pass filter characteristic with a low-frequency cut-off starting at as low as 20 Hz. For $R_{IN}=5.1$ kΩ, the input capacitance can be calculated as

$$C_{IN}=1/(2\pi f_{low}R_{IN})=1.5\ \mu\text{F}. \tag{22}$$

4 Results and discussions

The NI Multisim circuit implementation results are summarised in Table 1. The NI Multisim software is able to generate practical computational performance levels since the actual component models are used. Due to the noise and signal attenuation problems, the class-D amplifiers cannot be realised using a breadboard, and so the commercial class-D amplifiers are all implemented with integrated circuits, e.g. 0.5 µm complementary metal oxide semiconductor process. The provided implementation circuits are a good replicate of the actual circuits and can be refined by the circuit practitioners to produce a final product.

It seems that in practical implementations, the gain γ should not be zero to increase switching frequency in the hysteretic comparator for good control performance. The provided results are obtained when $\gamma=0.6$. To measure the output signal quality, total harmonic distortion (THD) is calculated using the harmonics calculated by fast Fourier transform with the following equation:

$$\text{THD(dB)}=20\log\left(\sqrt{H_2^2+\cdots+H_k^2}/H_1\right), \tag{23}$$

where H_k represents the harmonics. For a sinusoidal reference signal, $V_r=0.2\sin(2\pi 10000t)$, the control performances are compared in terms of THD, phase delay and amplification factor (gain). The calculated THD is around −48 dB for most of the controlled class-D amplifiers (it is calculated as low as −80 dB in numerical simulations).

Phase delay between reference and output signals is dependent on the degree of the system and can be calculated through $\phi=2\pi f t_d$ (rad) in time responses or $\phi\simeq\Delta V/V_{pp}$ (rad) in V_r versus V_{out} plot (Lissajous curves), where V_{pp} is the peak-to-peak voltage. In the following simulations and realisations, it is shown that the current feedback based control significantly decreases the phase delay between the reference and output signals, and provides a full scale amplification.

Numerical simulation results are obtained using MATLAB/ Simulink when $\gamma=0$, and illustrated in Figs. 4–6. For a sinusoidal reference signal, $V_r=0.2\sin(2\pi 10000t)$, the initial system responses are given for 200 µs. Both sensorless (method 1) and current feedback based (method 2) controllers provide a good tracking performance, with around a gain factor of 10. The current feedback based control decreases the phase delay more than 50% compared with the sensorless control. The numerical simulations are obtained for ideal elements and theoretically infinite switching frequency, which results in very small variations on the amplitude of the inductor current I_1. The average control signal is obtained through a first-order low pass filter whose time constant is of 5 µs. It also shows the gain and phase differences of the controllers.

In Fig. 5, the Lissajous curves of the controlled system responses are illustrated, which allows seeing the phase

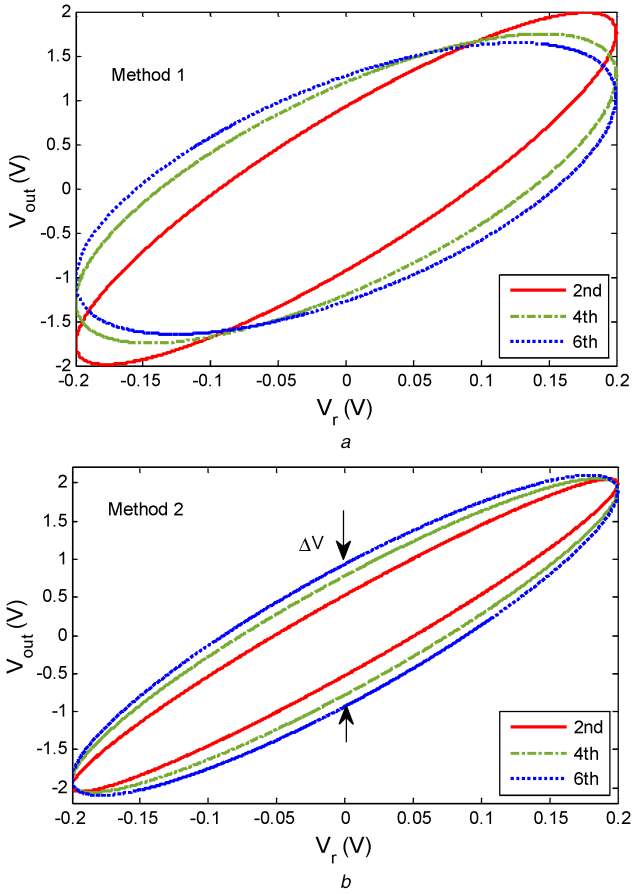

Fig. 5 *Numerical Lissajous curves*
(a) Sensorless control, ***(b)*** current feedback based control

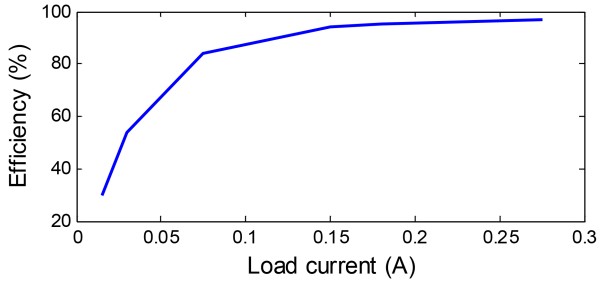

Fig. 6 *Load current based efficiency calculation*

relationship between the input/output waves. The phase delay can be calculated by $\phi \simeq \Delta V / V_{pp}$ (in rad). As amplifier order increases, the phase delay increases. As explained above, the current feedback based control yields much smaller phased delay compared with sensorless control. The gain (V_{out}/V_{in}) of the amplifier is taken as 10, and this gain is achieved with current based control (method 2), while the sensorless control provides slightly smaller gain in numerical simulations as seen in the figures.

The efficiency of the class-D amplifier under the proposed controllers is calculated from MATLAB SimPowerSystems simulations, and shown in Fig. 6. The figure is given for the fourth-order class-D amplifiers. The efficiency is dependent on input signal frequency, output voltage amplitude, and switching frequency. Here, a load current based efficiency plot is provided as an illustration, and it shows that the amplifier is more efficient at large loads while suffering at very light loads. The sensorless and current feedback based control methods provide very close results.

The control circuit schematics provided by Figs. 2 and 3 are realised with NI Multisim software, and the circuit realisation results are shown in Figs. 7–11. Fig. 7 shows the circuit waveforms for the sensorless control. As the amplifier order increases, the phase delay increases and the amplification factor (gain)

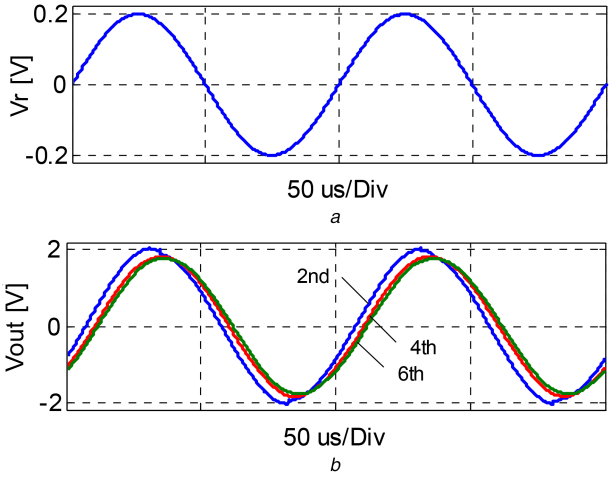

Fig. 7 *Sensorless control circuit waveforms*
(a) Reference input, ***(b)*** voltage output for second-, fourth- and sixth-order amplifiers

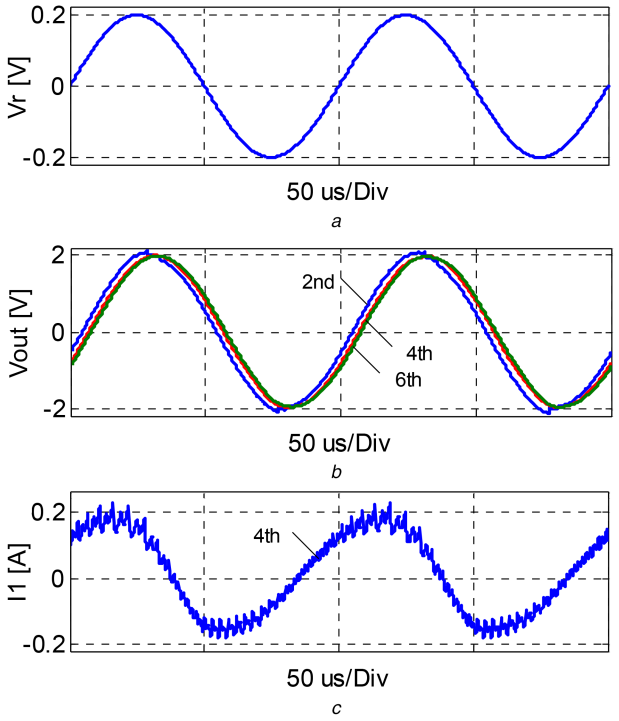

Fig. 8 *Current feedback based control circuit waveforms*
(a) Reference input, ***(b)*** voltage output for second-, fourth- and sixth-order amplifiers, ***(c)*** Inductor current for fourth-order amplifier

remarkably decreases, while the voltage output becomes smoother. The amplifier gain is set to be 10, and it is given as percentage (%) in Table 1.

Current feedback based control circuit results are shown in Fig. 8. Compared to sensorless control, the amplification factor stays constant and smaller phase delays are seen. Due to the implementation of the controller with a hysteretic comparator, the hysteretic variation in the inductor current is clearly observed in Fig. 8*c*.

The Lissajous curves of the circuit realisation results are illustrated in Fig. 9 for high-order class-D amplifiers. The current feedback based controller (Method 2) provides much smaller phase delay, which is compatible with the numerical simulations. In addition, the symmetry between input and output is almost lost with sensorless control, but the symmetry is preserved with the current feedback control with increasing system order. That is, the amplification factor of the sensorless control deteriorates with increasing system order, while the current feedback based control provides an excellent amplification factor.

Fig. 10 shows the discrete Fourier transform based power spectral density of the output of the fourth order class-D amplifier.

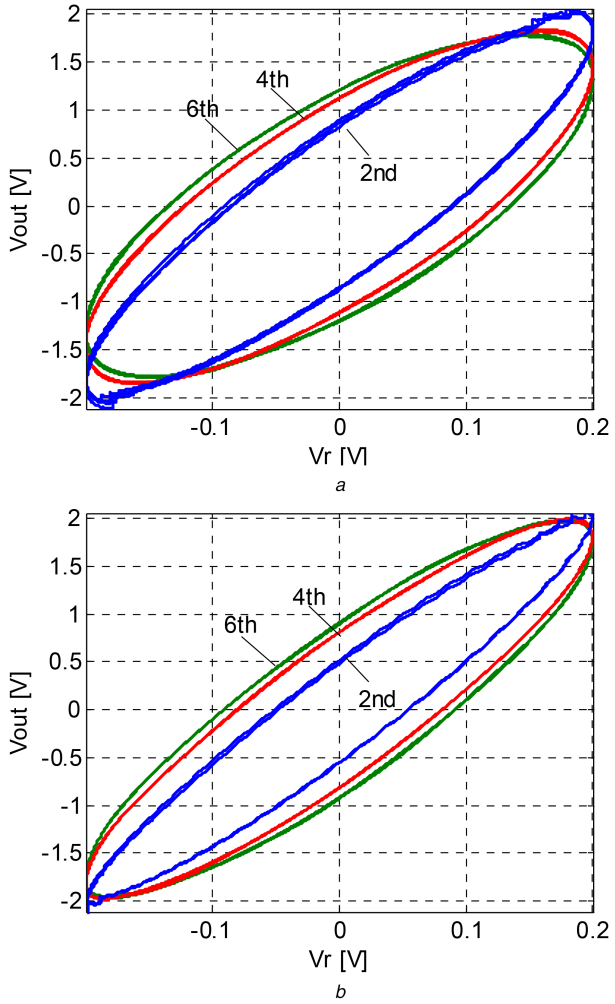

Fig. 9 *Circuit Lissajous curves for*
(a) Sensorless control, ***(b)*** Current feedback based control

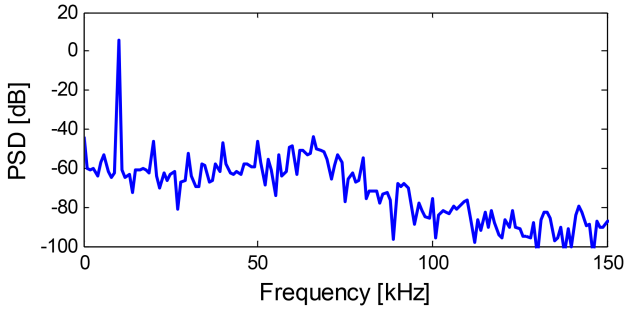

Fig. 10 *Power spectral density for the fourth-order amplifier under current feedback control*

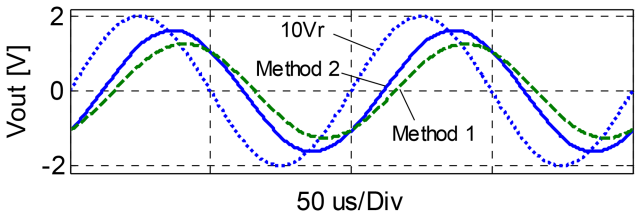

Fig. 11 *Responses of fourth-order amplifiers for a 4 Ω load*

The fundamental frequency of 10 kHz is clearly dominant compared with harmonics. The first five to ten harmonics are used to calculate THD of the output signal and provided in Table 1.

To measure the robustness of the integral controllers under load variations, the load resistance is changed from 8 to 4 Ω, and the tracking performances of controllers for the fourth-order class-D amplifier are shown in Fig. 11. The circuit results show that the amplifier output follows the reference input, but with a degradation in the amplification factor. The current feedback based control (Method 2) yields a better performance.

Note that in the literature, the available class-D amplifier controllers are given for second-order class-D amplifiers and are mostly based on circuit designs, rather than control theory based designs. In this work, the focus is on the theoretical control design, analysis and implementation of controllers for the high-order class-D amplifiers. For these reasons, a comparison with previous techniques is not provided since a direct and fair comparison is not possible.

5 Conclusion

Robust sensorless and current mode integral controllers for *n*th order class-D power amplifiers are investigated. The variable structure control theory is applied to establish the theoretical design and analysis of these non-linear controllers. The efficiency and feasibility of the controllers are verified with numerical simulations and circuit implementations. The sensorless control has a very simple implementation structure without any stability constraint, while current feedback based control improves the class-D power amplifier performance by reducing phase delay significantly and keeping amplification factor (gain) of the power amplifier at maximum. It is also shown that the proposed controllers ensure fast dynamic responses with small phase shifts with negligible steady-state errors and robustness against load variations.

6 References

[1] Berkhout, M., Dooper, L.: 'Class-D audio amplifiers in mobile applications', *IEEE Trans. Circuits Syst. Regul. Pap.*, 2010, **57**, (5), pp. 992–1002

[2] Kang, Y., Ge, T., He, H., *et al.*: 'A review of audio class D amplifiers'. Int. Symp. on Integrated Circuits (ISIC), Singapore, December 2016, pp. 1–4

[3] Chang, C.M., Wu, J.T.: 'A 95-dBA DR digital audio class-D amplifier using a calibrated digital-to-pulse converter', *IEEE Trans. Circuits Syst. Regul. Pap.*, 2017, **64**, (5), pp. 1106–1117

[4] Tu, Y.J., Jong, T.L., Liaw, C.M.: 'Development of a class-D audio amplifier with switch mode rectifier front-end and its waveform control', *IET Power Electron.*, 2011, **4**, (9), pp. 1002–1014

[5] Wang, M., Jiang, X., Song, J., *et al.*: 'A 120 dB dynamic range 400 mW class-D speaker driver with fourth-order PWM modulator', *IEEE J. Solid-State Circuits*, 2010, **45**, (8), pp. 1427–1435

[6] Kovačević, S., Pešić-Brđanin, T., Galić, J.: 'Intermodulation distortion of class D audio amplifier using pulse density modulation'. Zooming Innovation in Consumer Electronics Int. Conf. (ZINC), Serbia, June 2016, pp. 46–49

[7] Noh, J., Lee, D., Jo, J.G., *et al.*: 'A class-D amplifier with pulse code modulated (PCM) digital input for digital hearing aid', *IEEE J. Solid-State Circuits*, 2013, **48**, (2), pp. 465–472

[8] Kuo, C.H., Lin, S.C.: 'A delta-sigma modulator-based class-D amplifier'. IEEE 5th Global Conf. on Consumer Electronics, Japan, October 2016, pp. 1–2

[9] Lam, C.K., Tan, M.T., Cox, S.M., *et al.*: 'Class-D amplifier power stage with PWM feedback loop', *IEEE Trans. Power Electron.*, 2013, **28**, (8), pp. 3870–3881

[10] Antunes, V.M.E., Pires, V.F., Silva, J.F.A.: 'Narrow pulse elimination PWM for multilevel digital audio power amplifiers using two cascaded H-bridges as a nine-level converter', *IEEE Trans. Power Electron.*, 2007, **22**, (2), pp. 425–434

[11] Pascual, C., Song, Z., Krein, P.T., *et al.*: 'High-fidelity PWM inverter for digital audio amplification: spectral analysis, real-time DSP implementation, and results', *IEEE Trans. Power Electron.*, 2003, **18**, (1), pp. 473–485

[12] Midya, P., Roeckner, B., Bergstedt, S.: 'Digital correction of PWM switching amplifiers', *IEEE Power Electron. Lett.*, 2004, **2**, (2), pp. 68–72

[13] Nielsen, K.: 'PEDEC-a novel pulse referenced control method for high quality digital PWM switching power amplification'. 29th Annual IEEE Power Electronics Specialists Conf., PESC'98, Japan, May 1998, vol. 1, pp. 200–207

[14] Poulsen, S., Andersen, M.A.E.: 'Hysteresis controller with constant switching frequency', *IEEE Trans. Consum. Electron.*, 2005, **51**, (2), pp. 688–693

[15] Lu, J., Gharpurey, R.: 'Design and analysis of a self-oscillating class D audio amplifier employing a hysteretic comparator', *IEEE J. Solid-State Circuits*, 2011, **46**, (10), pp. 2336–2349

[16] Putzeys, B.: 'Simple self-oscillating class D amplifier with full output filter control'. 118th Audio Engineering Society Convention, Barcelona, Spain, May 2005, pp. 1–8

[17] Guo, L., Ge, T., Chang, J.S.: 'A 101 dB PSRR, 0.0027% THD + N and 94% power-efficiency filterless class D amplifier', *IEEE J. Solid-State Circuits*, 2014, **49**, (11), pp. 2608–2617

[18] Gaalaas, E., Liu, B.Y., Nishimura, N.: 'Integrated stereo delta-sigma class D amplifier'. IEEE Int. Solid-State Circuits Conf., CA, USA, February 2005, pp. 120–588

[19] Kang, K., Roh, J., Choi, Y.*, et al.*: 'Class-D audio amplifier using 1-bit fourth-order delta-sigma modulation', *IEEE Trans. Circuits Syst. II Express Briefs*, 2008, **55**, (8), pp. 728–732
[20] Jung, S.-H., Kim, N.-I., Cho, G.-H.: 'Class D audio power amplifier with fine hysteresis control', *Electron. Lett.*, 2002, **38**, (22), pp. 1302–1303
[21] Lu, J., Gharpurey, R.: 'A self oscillating class D audio amplifier with 0.0012% THD + N and 116.5 dB dynamic range'. IEEE Custom Integrated Circuits Conf. (CICC), CA, USA, September 2010, pp. 1–4
[22] Ge, T., Chang, J.S.: 'Bang-bang control class D amplifiers: total harmonic distortion and supply noise', *IEEE Trans. Circuits Syst. Regul. Pap.*, 2009, **56**, (10), pp. 2353–2361
[23] Silva, J.F.: 'PWM audio power amplifiers: sigma delta versus sliding mode control'. IEEE Int. Conf. on Electronics, Circuits and Systems, Portugal, September 1998, pp. 359–362
[24] Rojas-Gonzalez, M.A., Sanchez-Sinencio, E.: 'Design of a class D audio amplifier IC using sliding mode control and negative feedback', *IEEE Trans. Consum. Electron.*, 2007, **53**, (2), pp. 609–617
[25] Yu, S.-H., Tseng, M.-H.: 'Use of sliding-mode modulation in switch-mode power amplification', *IEEE Trans. Ind. Electron.*, 2008, **55**, (11), pp. 4022–4028
[26] Torres, J., Colli-Menchi, A., Rojas-Gonzalez, M.A.*, et al.*: 'A low-power high-PSRR clock-free current-controlled class-D audio amplifier', *IEEE J. Solid-State Circuits*, 2011, **46**, (7), pp. 1553–1561
[27] Ablay, G.: 'Robust tracking controller for SEPIC drivers', *Electron. Lett.*, 2016, **52**, (24), pp. 2007–2009
[28] Utkin, V.I., Guldner, J., Shi, J.: '*Sliding mode control in electromechanical systems*' (CRC Press, Boca Raton, 2009)
[29] Williams, A., Taylor, F.: '*Electronic filter design handbook*' (McGraw Hill Professional, New York, 2006, 4th edn.)